DISCLAIMER

Visible-Light Photoredox Catalysis: Selective Reduction of Carbon Dioxide to Carbon Monoxide by a Nickel *N*-Heterocyclic Carbene-Isoquinoline Complex

V. Sara Thoi,[1,4,6] Nikolay Kornienko,[1,6] Charles G. Margarit,[1] Peidong Yang,[1,5] & Christopher J. Chang*[1-4]

[1]Departments of Chemistry and [2]Molecular and Cell Biology and the [3]Howard Hughes Medical Institute, University of California, Berkeley, California 94720, United States

[4]Chemical Sciences Division and [5]Materials Sciences Division, Lawrence Berkeley National Laboratory, Berkeley, California 94720, United States

[6]These authors contributed equally to this work

chrischang@berkeley.edu

ABSTRACT: The solar-driven reduction of carbon dioxide to value-added chemical fuels is a longstanding challenge in the fields of catalysis, energy science, and green chemistry. In order to develop effective CO_2 fixation, several key considerations must be balanced, including: (1) catalyst selectivity for promoting CO_2 reduction over competing hydrogen generation from proton reduction, (2) visible-light harvesting that matches the solar spectrum, and (3) the use of cheap and earth-abundant catalytic components. In this report, we present the synthesis and characterization of a new family of earth-abundant nickel complexes supported by *N*-heterocyclic carbene-amine ligands that exhibit high selectivity and activity for the electrocatalytic and photocatalytic conversion of CO_2 to CO. Systematic changes in the carbene and amine donors of the ligand have been surveyed, and $[Ni(^{Pr}bimiq1)]^{2+}$ (where ^{Pr}bimiq1 = bis(3-(imidazolyl)isoquinolinyl)propane, **1c**) emerges as a catalyst for electrochemical reduction of CO_2 with the lowest cathodic onset potential (E_{cat} = −1.2 V vs. SCE). Using this earth-abundant catalyst with $Ir(ppy)_3$ (where ppy = 2-phenylpyridine) and an electron donor, we have developed a visible-light photoredox system for the catalytic conversion of CO_2 to CO that proceeds with high selectivity and activity and achieves turnover numbers and turnover frequencies reaching 98,000 and 3.9 s^{-1}, respectively. Further studies reveal that the overall efficiency of this solar-to-fuel cycle may be limited by the formation of the active Ni catalyst and/or the chemical reduction of CO_2 to CO at the reduced nickel center and provide a starting point for improved photoredox systems for sustainable carbon-neutral energy conversion.

Introduction

The search for sustainable resources has attracted broad interest in the potential use of carbon dioxide as a feedstock for fuels and fine chemicals.[1-10] In this context, the photocatalytic reduction of CO_2 is an attractive route that can take advantage of the renewable and abundant energy of the sun for long-term CO_2 utilization,[6,11-13] with the eventual target of coupling the reductive half-reaction of CO_2 fixation with a matched oxidative half-reaction such as water oxidation to achieve a carbon-neutral artificial photosynthesis cycle.[14-21] Before this ultimate goal can be realized, however, a host of basic scientific challenges must be addressed, including developing systems that balance selectivity, efficiency, and cost. With regard to selectivity, it is critical to minimize the competitive reduction of water to hydrogen that is typically kinetically favored over CO_2 reduction, as well as selectively convert CO_2 to one carbon product.[22,23] Another primary consideration is the use of visible-light excitation, which more effectively harvests the solar spectrum and avoids deleterious high-energy photochemical pathways. Semiconductors such as TiO_2 and SiC have been widely employed as heterogeneous catalysts for photochemical and photoelectrochemical conversion of CO_2 to a variety of carbon products such as carbon monoxide, methanol, and methane.[12,13] However, examples of selective light-driven CO_2 conversion to reduced carbon products in heterogeneous systems are limited mainly to these wide-band gap, UV-absorbing materials that do not exhibit selectivity towards a single carbon product,[24-27] aside from select transition-metal doped silicates.[28-30] The use of semiconductors with molecular electrocatalysts has also been investigated for photoelectrochemical CO_2 conversion,[31-33] and recent work in improved inorganic materials for electrocatalytic CO_2 reduction continues to emerge,[34-40] but limited photocatalytic applications have been reported.

Homogeneous molecular systems offer an alternative strategy for solar CO_2 fixation that allows for modular tuning of their performances via synthetic chemistry. However, most CO_2 reduction efforts in this context have focused on electrocatalysts, including those based on cobalt and nickel polyamine macrocycles,[41-47] second- and third-row transition metal polypyridines,[48-58] metal porphyrins[59-62] and phthalocyanines,[63-65] metal phosphines[3,66-69] and thiolates,[70] metal clusters,[71] pyridine and amine derivatives,[72-75] and *N*-heterocyclic carbene-pyridine platforms.[76] To date, no one synthetic system combines visible-light excitation and earth-abundant metal catalysts to achieve sustainable, solar CO_2 conversion to a predominant product with high selectivity and activity. For example, photochemical reductions of CO_2 with selective product formation using rhenium polypyridine catalysts have been extensively investigated, but these third-row transition metal photosensitizers absorb largely in the UV region and do not utilize the full solar spectrum.[77,78] UV-excitable organic photosensitizers, such as *p*-terphenyl[79-81] and phenazine,[82] have also been used for photochemical CO_2 fixation.

Visible-light photocatalytic CO_2 reduction has been largely limited to noble-metal catalysts that achieve low turnover numbers and/or selectivity. For instance, $[Ru(bpy)_3]^{2+}$ can be used as both a photosensitizer and a catalyst for reducing CO_2 to formate with turnover numbers (TONs) reaching up to 27 within 24 h.[83] Related systems with $[Ru(bpy)_3]^{2+}$ as a photosensitizer and $Re(bpy)(CO)_3Cl$ have reported TONs reaching up to 48 in 4 h for selective CO production.[48] First-row transition metal complexes have also been used in conjunction with $[Ru(bpy)_3]^{2+}$; early work on nickel N_4-macrocycles and $[Ru(bpy)_3]^{2+}$ have been demonstrated to approach TONs of 0.1 for CO production, but with concomitant H_2 production with TONs up to 0.7.[84,85] Such undesirable proton reduction pathways are also observed in cobalt-based systems with $[Ru(bpy)_3]^{2+}$, where CO/H_2 ratios typically range between 0 to 3, with optimized CO/H_2 ratios of up to 19 resulting in markedly lower overall CO and H_2 production.[86,87] Multinuclear bipyridine-based Ru-Re[88,89] and Ru-Ru[90] complexes can also reduce CO_2 to CO and formic acid, respectively. More recently, a series of Ir(tpy)(R-ppy)Cl complexes (where tpy = terpyridine, ppy = phenylpyridine, R = H, Me) that absorb visible light have been reported to reduce CO_2 to CO photocatalytically with TONs of up to 50 within 5 h.[91] Moreover, in the aforementioned cases, high-power 500 W to 1000 W Xe or Xe-Hg lamps are typically necessary to achieve the reported turnover numbers, noting that values for power per area are not noted. Since the average solar intensity is measured to be around 136.6 $mW \cdot cm^{-2}$,[92,93] low-intensity light would be advantageous for more practical application of these technologies.

Against this backdrop, we have initiated a program aimed at developing visible-light photoredox systems using earth-abundant catalysts for the selective conversion of CO_2 to value-added products. Inspired by the seminal $[Ni(cyclam)]^{2+}$ complex (where cyclam = 1,4,8,11-tetraazacyclotetradecane) and related systems that exhibit high selectivity for reducing CO_2 over H_2O[1,41-43,45,46,58,80,94] and the rapid emergence of visible-light photoredox catalysis for organic transformations,[95-100] we sought to couple visible-light photosensitizers of appropriate reducing power with first-row transition metal catalysts to drive CO_2 fixation chemistry at earth-abundant metal centers. We now report the synthesis, properties, and evaluation of a new family of nickel complexes supported by *N*-heterocyclic carbene-amine ligands that can perform both electrocatalytic and photocatalytic carbon dioxide reduction with high selectivity over proton reduction. Through systematic substitutions on the ancillary donors, we have discovered a nickel *N*-heterocyclic carbene-isoquinoline platform that achieves visible-light catalytic photoredox conversion of CO_2 selectively to CO with no detectable formation of hydrogen from off-pathway proton reduction processes. Using a relatively low-power 150 W Xe lamp that corresponds to 130 $mW \cdot cm^{-2}$ under our experimental conditions, we achieve TONs and turnover frequencies (TOFs) approaching 98,000 and 3.9 s^{-1}, respectively. Further experiments reveal that the catalytic activity in this photoredox cycle is limited by either the formation of the active nickel catalyst or the chemical conversion of CO_2 to CO, providing a path forward for future designs of carbon-neutral solar-to-fuel conversion processes based on this strategy.

Results and Discussion

Synthesis and Characterization of a Homologous Family of Nickel *N*-Heterocyclic Carbene-Amine Complexes Bearing Benzimidazole-Based Carbene Donors or Isoquinoline Amine Donors. Based on precedent with $[Ni(cyclam)]^{2+}$ and related N_4 macrocyclic systems that exhibit high selectivity for reducing CO_2 over H_2O under electrocatalytic conditions,[1,40-44,54,79,91] we reasoned that developing new planar, electron-rich platforms with a d_{z^2}-based nucleophile would provide a good starting point for investigation. To this end, we previously communicated a trio of nickel complexes supported by *N*-heterocyclic carbene-pyridine ligands that demonstrated adjustments in the length of the bridgehead tether to offer tunability of cathodic reduction potentials.[76] Although these first-generation systems are capable of highly selective electrochemical reduction of CO_2 over H_2O, they are limited by their modest catalytic activity and long-term stability. To address these shortcomings, we designed and synthesized a new family of nickel catalysts with systematic changes at the *N*-heterocyclic carbene and amine donors (Scheme 1). Using the modular synthetic approach outlined in Scheme 2, building blocks **1a**-**3a** were synthesized by a palladium- or copper-catalyzed carbon-nitrogen coupling of an imidazole or benzimidazole precursor and a halogenated pyridine or isoquinoline.[101] The respective bis-*N*-heterocyclic carbene-amine ligands **1b**-**3b** can be readily prepared by alkylation of **1a**-**3a** with the appropriate dihalide linker. For example, alkylation of **1a** by dibromopropane, followed by an anion exchange with NH_4PF_6, afforded ligand **1b**. In addition, the effects of conjugation on CO_2 reduction can be interrogated by the synthesis and characterization of bis(2-benzimidazolylmethylpyridine)propane hexafluorophosphate (**4b**), which contains extra methylene groups that break the π system between the *N*-heterocyclic carbene and the pyridine donors. Deprotonation of the ligands by Ag_2O followed by metallation with $Ni(DME)Cl_2$ yielded the chloride-bound nickel complexes, which were then treated with $NaPF_6$ to afford the final catalysts **1c**-**4c** in near-quantitative yield. As expected, all four complexes are diamagnetic as shown by ^1H and ^{13}C NMR measurements.

The solid state structures of **1c**-**4c** determined from single-crystal X-ray crystallography are shown in Figure 1. In line with our previous work on tuning alkyl linkers in the Ni(^{R}bimpy) series,[76] the propyl bridge allows a great degree of flexibility and the four-coordinate nickel centers in all four complexes display distorted square-planar geometries. This distortion is quantified by measuring the torsion angle formed by N_{amine}-Ni-N_{amine}-C_{ortho} in the complexes, and these angles range from 24.7° to 57.2 (Figure 1). The Ni-N and Ni-C bond lengths are within the typical range for these types of donors.[76,102-104]

Evaluation of Nickel *N*-Heterocyclic Carbene-Amine Complexes for Electrocatalytic CO_2 Reduction. The electrochemical behaviors of complexes **1c**-**4c** were interrogated by cyclic voltammetry. First, the electronic effects of the extended conjugation on the carbene and amine donors of the ligand scaffold were examined (e.g., isoquinoline for pyridine, benzimidazole for imidazole). The cyclic voltammogram of an acetonitrile solution of quinoline-based **1c** and 0.1 M NBu_4PF_6 electrolyte exhibits two reversible reductions at $E_{1/2}$ = –0.92 V and –1.38 V vs. SCE under a nitrogen atmosphere (Figure 2a). For comparison, the cyclic voltammogram of quinoline-based **2c**, in which the *N*-heterocyclic carbene is substituted at the 1-position of the isoquinoline ligand, displays two reversible reductive processes at $E_{1/2}$= –0.74 V, –1.20 V and an irreversible process at E_{pc} = –1.60 V under N_2 (Figure 2b). Under a CO_2 atmosphere, the cyclic voltammograms of both complexes **1c** and **2c** show enhanced current at E_{onset} = –1.20 V and –1.40 V, respectively, which is indicative of electrocatalysis. Notably, catalyst **1c** represents a marked improvement in overpotential compared to the parent complex $[Ni(^{Pr}bimpy)](PF_6)_2$, which exhibits a cathodic catalytic current for reducing CO_2 at E_{onset} = –1.40 V. In contrast to what is observed for complexes **1c** and **2c** where the conjugation is extended by using an isoquinoline donor, extending the conjugation on the imidazole-based *N*-heterocyclic carbene donor with a benzimidazole carbene shifts the onset reduction potential for CO_2 reduction to more negative values. Indeed, the cyclic voltammogram of **3c** features two reversible reductions at $E_{1/2}$ = –0.63 V and –1.22 V vs. SCE (Figure 2c) under a nitrogen atmosphere and enhanced current at E_{onset} = –1.47 V under a CO_2 atmosphere.

Breaking the conjugation between the *N*-heterocyclic carbene and the amine donors also shifts the onset potential of CO_2 reduction to more negative values. For example, the cyclic voltammogram of **4c** displays two irreversible processes at E_{pc} = –1.10 V and –1.43 V under N_2 with only a slight current enhancement at E_{onset} = –1.45 V under CO_2 (Figure 3a). As a result of the larger chelate ring size around the Ni center, the steric strain in **4c** is expected to be higher than in the case of **3c**. Indeed, this strain is reflected in the differences in the torsion angles along N_{Py}-Ni-N_{Py}-C_{ortho} core between **3c** and **4c**; the extra methylene groups between the pyridine and carbene cause the observed torsion angle in **4c** (57.2°) to be much larger than that of **3c** (24.7°). We further probed the extent of these strain effects on CO_2 reduction by evaluating an analogous nickel *N*-heterocyclic carbene-pyridine complex previously synthesized by Chen and co-workers (**5c**),[102] which contains a methylene bridge between the *N*-heterocyclic carbenes in place of the propyl linker in **4c**. This small change leads to a decreased torsion angle of 45.1° along N_{Py}-Ni-N_{Py}-C_{ortho} core. As anticipated, the cyclic voltammogram of **5c** shows two irreversible reductions at E_{pc} = –1.02 V and –1.56 V under an N_2 atmosphere with only a modest current enhancement at E_{onset} = –1.50 V upon addition of CO_2 (Figure 3b). Both **4c** and **5c** are significantly less active than **1c**-**3c** towards CO_2 reduction, suggesting that the extended conjugation at the appropriate location on the ligand platform is favorable for catalytic CO_2 reduction.

By systematically tuning the location and type of ligand conjugation in this series of nickel complexes, catalyst **1c** is determined to have the lowest overpotential for CO_2 reduction potential at E_{onset} = –1.20 V. Controlled-potential electrolysis of an acetonitrile solution of 0.02 mM of **1c** in the presence of 0.1 M NBu_4PF_6 at E_{cat} = –1.80 V vs. SCE was conducted over an 8-h period (Figure S3). The headspace was analyzed by gas chromatography in 30-min intervals and CO was detected as the major gas product (Figure 4), along with trace amounts of CH_4 (Figure S4). The Faradaic efficiency (FE) for CO production is 90% with no detectable formation of hydrogen within the first 30 min. A total turnover number (TON) of 35 and an endpoint FE of 22% are calculated for CO production at 8 h (Figure S5). No other gas or solution products are detected through GC or NMR analysis. We speculate that the decrease in FE from 90% within the first 30 min to 22% at 8 h may be attributed to the re-oxidation of CO_2-reduced products at the counter electrode as they accumulate in the reactor; in this case, we anticipate that FE could be improved through reduced mass transfer of CO_2-reduced products between the working electrode and counter electrode compartments. Indeed, this mass transfer issue is solved through the use of a photoredox cycle with an external quencher, which achieves much higher activity, selectivity, and long-term stability.

Development a Solar-driven Photoredox Cycle for Catalytic CO_2 Reduction with Nickel *N*-Heterocyclic Carbene-Isoquinoline Complex 1c. With electrochemical data showing that improvements in overpotential, we moved to incorporate molecular catalyst **1c** into a solar-driven photoredox cycle for CO_2 reduction. Specifically, we sought to combine this earth-abundant CO_2 catalyst with an appropriate light absorber that could subsequently transfer a high-energy electron to the nickel center. An iridium photosensitizer supported by *fac*-tris(phenylpyridine), $Ir(ppy)_3$, was selected owing to its ability to absorb solar photons in the visible region[92,93] (Figure S6) and potentially large driving force for the subsequent reduction of the nickel catalyst.[105,106]

A series of experiments were conducted to test the viability of using catalyst **1c** combined with the visible-light absorber $Ir(ppy)_3$ and a sacrificial reductant, triethylamine (TEA), in a photoredox cycle for CO_2 reduction. Typical photolysis experiments were conducted with a 130 $mW \cdot cm^{-2}$ Xe lamp equipped with an AM 1.5 filter to simulate the solar spectrum and intensity. A glass bubbler containing an acetonitrile solution containing CO_2 (~0.28 M), catalyst, photosensitizer, and quencher was illuminated and the headspace was directly analyzed by GC every hour. As shown in Figure 5, the visible-light photoredox cycle produced a significant amount of CO product over background, along with trace amounts of CH_4 and C_2H_4 (Figure S7), with activity that persisted for at least 7 h. Moreover, no hydrogen was observed above the detection limit of 1 ppm, establishing the high selectivity of this photoredox system for CO_2 over proton reduction. Table 1 summarizes the TONs and TOFs under a variety of conditions. At 200 nM of catalyst **1c** and 0.2 mM $Ir(ppy)_3$, the TON and TOF values are 1,500 and 0.058 s^{-1}, respectively, using the CO product quantified after 7 h of photolysis. Moreover, TONs and TOFs as

high as 98,000 and 3.9 s^{-1}, respectively are determined using 2 nM loadings of **1c**. The high turnover values achieved using this earth-abundant catalyst under visible-light photoredox conditions establish its promise for potential larger-scale CO production cycles.

A number of control experiments were performed to establish that all molecular components are necessary for the observed solar-to-fuel catalysis. First, negligible CO product was detected in an illuminated acetonitrile solution containing only 0.2 mM $Ir(ppy)_3$ photosensitizer and 0.07 M TEA in the absence of catalyst **1c.** Additionally, solutions containing the simple nickel salt $[Ni(MeCN)_6]^{2+}$ or the free ligand **1b** did not produce comparable activity to the nickel complex **1c**. Control experiments without photosensitizer or quencher also showed negligible CO generation under photochemical irradiation, and no CO was produced in a dark reaction with all components added. To ascertain if heterogeneous particles were formed during photolysis, transmission electron microscopy (TEM) experiments were conducted on the samples before and after photolysis. Samples were prepared by drop-casting 100 μL of solution onto a thin film copper or molybdenum TEM grid and the grid was allowed to completely dry before loading into the instrument. The TEM images between samples pre- and post-photolysis are similar (Figure S8), and several energy dispersive spectroscopy (EDS) measurements over large areas of the samples show no detectable Ir and Ni content at the sensitivity limit of this experiment (<0.5 atomic %). Taken together, these supporting data suggest involvement of a molecular nickel species in the observed photocatalysis.

Characterization of the Visible-Light Photoredox Cycle for Catalytic CO_2 Reduction. We next sought to probe various aspects of the photoredox cycle for catalytic CO_2 reduction mediated by nickel complex **1c**. First, the quantum efficiency (QE) of the overall catalytic photoredox cycle for CO_2 reduction is determined by using the following equation:

$$QE = \frac{CO\,molecules \times 2}{Incident\,Photons} * 100\%$$

Here, the number of incident photons can be calculated from the incident photon flux of 1.2×10^{21} photons·cm^2·h^{-1} (at 130 mW·cm^{-2}) and an illuminated area of 4.24 cm^2. The molecules of CO generated are then back-calculated from the concentration of CO (in ppm) and the total volume of the system (80 mL); after 7 h of photolysis, 2.1×10^{-5} mol of CO is produced. The calculated quantum yield for this visible-light molecular photosensitizer system is 0.01%, which is two orders of magnitude higher than that achieved using illuminated semiconductor powders.[107,108]

In an attempt to improve upon this yield, we varied the solar intensity under photoredox conditions. As plotted in Figure 6, the CO production rate increases almost linearly up to illumination intensities of 50 mW·cm^{-2} (which corresponds to an incident photon flux of approximately 1.32×10^{17} photons·s^{-1}). We observe that the CO production levels off with illumination intensities above this value, suggesting that the CO production rate is not limited by the light absorption past this point and that another step in the photoredox cycle is limiting the overall solar-to-fuel conversion efficiency. Furthermore, the relatively low intensity of light used in the current photoredox system may be advantageous for conditions in which solar flux is limiting, such as when direct sunlight is not available.

We next examined the dependence of photosensitizer concentration on CO production by varying the concentration of $Ir(ppy)_3$ from 2 μM to 200 μM while maintaining the concentration of catalyst **1c** at 200 nM and keeping all other reaction parameters constant. A plot of moles of CO product generated versus photosensitizer concentration shows a clear first-order dependence on $Ir(ppy)_3$ concentration (Figure 7). Similar experiments were performed where the concentration of **1c** was varied. However, extracting useful kinetic information proved to be more elusive in this case. Although patent differences in the rates of CO product formation are observed when the catalyst concentration is varied between 0 and 200 nM, there are similar rates of product formation at 2 and 20 nM catalyst loading within experimental error (Figure S9). We speculate that this peculiar dependence may indicate a change in mechanism, as the concentration of the catalyst varies between 10- and 10^3-fold less than the photosensitizer and between 10^3- and 10^6-fold less than the quencher; this open question will be a subject of future studies.

To probe the mechanism of photoinduced electron transfer in this catalytic system further, we examined the rate of quenching of the $Ir(ppy)_3$ excited state by the catalyst and by the electron donor, TEA, under our photocatalytic conditions using Stern-Volmer analysis according to the following equation:

$$\frac{I_0}{I} = 1 + k_q \tau_0 [Q]$$

In this equation, I_0 and I are the fluorescence intensity in the absence and presence of the quencher, k_q is the apparent rate of quenching, τ_0 is the lifetime of the excited state, and [Q] is the concentration of the quencher. At an excitation wavelength of 400 nm, the fluorescence intensity at 517 nm for the $Ir(ppy)_3$ lumophore was plotted against varying concentrations of catalyst **1c** to give an apparent quenching rate constant of 1.7×10^9 s^{-1} (Figure 8). For comparison, typical rate constants for quenching of $[Ru(bpy)_3]^{2+}$* are on the order of 10^7-10^{10} s^{-1},[109] suggesting that direct oxidative quenching of the $Ir(ppy)_3$ with the catalyst can reasonably operate in this photocatalytic system. As further evidence for an oxidative quenching mechanism, the fluorescence of $Ir(ppy)_3$ is not attenuated when TEA alone was used as the quencher (Figure 8c).

Finally, we examined the role of the sacrificial reductant in the photoredox catalysis cycle. Oxidation of triethylamine by $[Ir(ppy)_3]^+$ generates an amine radical, which can potentially act as an oxygen atom acceptor and form the *N*-oxide, diethylamine, and acetaldehyde.[110] We also screened a series of other electron donors (Figure S10). Using a standard set of conditions (0.2 mM $Ir(ppy)_3$, 0.2 μM **1c**, and 0.07 M of the sacrificial reductant), we observed total CO production at 7 h increasing in the following order: isopropanol (IPA) < triethanolamine (TEOA) < dimethylaminoethanol (DMAE) < triethylamine (TEA). These results confirm the importance of the quencher in the photoredox system and may suggest that the ability of the sacrificial reductant to accept oxygen atoms can impact CO_2 reduction. For the realization of large scale CO_2 reduction using this system, a more economic sacrificial reductant such as sulfite or ascorbic acid may be used in a solubilizing solvent.

Implications for Design of Improved Photoredox Systems for Catalytic CO_2 Reduction. In addition to establishing an active and selective visible-light photoredox cycle for catalytic reduction of CO_2 to CO, the aforementioned results have implications for the future design of improved systems for solar-to-fuel conversion. Scheme 3 summarizes a potential set of reactions occurring during the photocatalytic reduction of CO_2 to CO. Upon illumination, $[Ir(ppy)_3]$ is excited to $[Ir(ppy)_3]$*, which is governed by the apparent rate constant k_1. The excited [Ir(ppy)]* is then quenched and, with a reduction potential of −1.73 V,[106] is oxidized by the nickel catalyst at an apparent k_q (composed of k_{q1} and k_{q2}) measured to be 1.7×10^9 s^{-1}. Since the first and second reduction potentials of **1c** are $E_{1/2}$ = –0.92 V and –1.38 V, the driving forces for generating the one- and two-electron reduced species are ca. 800 mV and 350 mV, respectively. The oxidized $[Ir(ppy)_3]^+$ is subsequently reduced by the sacrificial reductant at a reduction potential of $E_{1/2}$ = 0.77 V to close the catalytic cycle (apparent k_2). Based on the electrochemical behavior of **1c**, we speculate that **1c** may be reduced twice via two one-electron transfers before being activated towards the two-electron reduction of CO_2 to CO (apparent k_{cat}). As the overall conversion efficiency in our system is limited by the slowest of these complex processes, we have systematically probed various reaction parameters directly associated with each of these processes to find the critical factors that can be improved in future designs.

Visible-light absorption by the photosensitizer is unlikely to be a limiting step under our reaction conditions as the CO production remains constant at illumination intensities greater than 50 $mW \cdot cm^{-2}$. The first-order dependence of CO production on the $Ir(ppy)_3$ photosensitizer concentration also suggests that k_1 is not rate-limiting. However, the identity of the sacrificial reductant does affect the production of CO and offers an alternative variable to tune for improvement. Based on these systematic experiments, we hypothesize that the rate-determining step is likely either CO_2 reduction at the nickel center (k_{cat}) or the reduction of **1c** to the active Ni catalyst by $[Ir(ppy)_3]$* (k_q), since two one-electron transfers from $[Ir(ppy)_3]$* to the Ni catalyst must occur for every one CO_2-to-CO transformation.

Finally, perhaps the most straightforward path forward for improvement is revealed by long-term stability measurements of the photocatalytic CO_2 reduction cycle. The observed rate of CO production remains linear over a time span of 7 h but plateaus after this time point. However, when a second equivalent of visible-light photosensitizer was injected into the solution after 13 h of continued photolysis, CO production resumed at a similar rate (Figure 9). This result suggests that degradation of the photosensitizer, rather than catalyst deactivation, is a limiting factor for extended CO_2 reduction. Developing photosensitizers with greater photostability and more efficient absorption of incident visible and near-infrared photons in the solar spectrum is a promising strategy to increase the long-term activity and efficiency of these solar-to-fuel conversion systems. Another direction is to increase the water-solubility or water-compatibility of the photosensitizer such that more economical electron donors such as sulfites and ascorbic acid can be employed.

Concluding Remarks

In summary, we have described the synthesis and characterization of a new family of nickel complexes supported by *N*-heterocyclic carbene-amine ligands and their application for electrocatalytic and photocatalytic reduction of CO_2 to CO. Focusing on *N*-heterocyclic carbene-isoquinoline complex **1c**, the most promising candidate in terms of cathodic onset potential, controlled potential electrolysis studies establish its utility as a CO_2-to-CO reduction catalyst with high selectivity over competing off-pathway proton-to-hydrogen reduction reactions. Using this molecular CO_2 reduction catalyst in conjunction with the photosensitizer $Ir(ppy)_3$, we have developed a visible-light photoredox system for the catalytic conversion of CO_2 to CO at a relevant solar intensity of 130 $mW \cdot cm^{-2}$. Solar-driven CO_2 reduction proceeds with TONs and TOFs reaching as high as 98,000 and 3.9 s^{-1}, respectively, with no detectable formation of hydrogen. The overall solar-to-fuel efficiency of 0.01% for this molecular system is two orders of magnitude higher than achieved using illuminated semiconductor powders. Experiments to probe various charge-transfer steps in this photoredox cycle reveal that the generation of the active Ni catalyst by [Ir(ppy)]* and the conversion of CO_2 to CO by the reduced nickel center are likely limiting steps. In addition to performing further ligand modifications to decrease overpotential and increase the rate of catalysis, current lines of investigation include optimizing electron transfer between photosensitizer and catalyst components, exploring molecular and solid-state photosensitizers with greater light-harvesting capabilities across the solar spectrum, translating this catalytic chemistry to environmentally benign aqueous media, and coupling this reductive light-driven half-reaction to an appropriate oxidative process to achieve a complete solar-to-fuel system.

Experimental Section

General Synthetic and Physical Methods. Unless noted otherwise, all manipulations were carried out at room temperature under ambient conditions. All reagents and solvents were purchased from commercial sources and used without further purification. Literature methods were used to synthesize $Ni(DME)Cl_2$,[111] 2-benzimidazolylmethylpyridine (**4a**),[102] and $[Ni(^{Me}bbimpic)](PF_6)_2$ (**5c**).[102] NMR spectra were recorded using Bruker spectrometers operating at 300, 400, or 500 MHz as noted. Chemical shifts are reported in ppm relative to residual protiated solvent; coupling constants are reported in Hz. High-resolution mass spectra were collected using a Finnigan LTQ FT (Thermo) and Autospec Premier (Waters) mass spectrometer using electrospray and electron impact ionization, respectively, at QB3 Mass Spectrometry Facility at University of California, Berkeley. Elemental analyses were conducted at the University of California, Berkeley Microanalytical Laboratory.

Electrochemistry. Non-aqueous electrochemical experiments were conducted under a N_2 or CO_2 atmosphere in 0.1 M NBu_4PF_6 in CH_3CN. Cyclic voltammetry experiments were carried out using BASI's Epsilon potentiostat and C-3 cell stand. The working electrode was a glassy carbon disk (3.0 mm diameter) and the counter electrode was a platinum wire. A silver wire in porous Vycor tip glass tube filled with 0.1 M NBu_4PF_6 in CH_3CN was used as a pseudo-reference electrode. The scan rate for all cyclic voltammograms was 100 $mV \cdot s^{-1}$. All potentials were referenced against ferrocene/ferrocenium as an external standard and converted to SCE by adding 0.40 V to the measured potentials.[112] Controlled-potential electrolysis experiments were carried out using BASI's Epsilon potentiostat in a custom-made Teflon two-compartment cell separated by a Nafion membrane. The cell is connected to a circulator and a SRI Gas Chromatograph for headspace analysis (Figure S1 and S2). A glassy carbon rod, a platinum wire, and a $Ag/AgNO_3$ reference electrode were used as the working, counter, and reference electrode, respectively. Typically, a 15 mL solution of 0.2 mM catalyst in 0.1 M NBu_4PF_6 in CH_3CN (from chemical supplier) was sparged for 30 min with N_2 or CO_2 and cyclic voltammograms were taken. The solution is electrolyzed at −1.8 V vs. SCE in 30-min intervals under CO_2 and gas products in the headspace are monitored by GC. After each 30-min electrolysis, a gas recirculation pump was used to homogenize the gas composition in the system for 60 s and was followed by a GC analysis of the headspace. Following the GC sampling, CO_2 was sparged through the system for 2 min to reach the saturation point of aqueous CO_2 solubility. Following this, the system was closed off and another chronoamperometric run was resumed.

Photocatalytic Studies. A 40-mL glass bubbler was used as the photochemical cell that was connected to a gas recirculation pump (Air Dimensions, B121-AP-AA1) and a SRI 8610C Gas Chromatograph (MG#3 pre-configuration) with a 2 m Haysep-D and a 2 m MolSieve 13X column leading to TCD and FID detectors (Figure S1 and S2). The FID detector was fitted with a methanizer to detect CO at a detection limit of 0.1 ppm and the TCD detector was used to detect H_2 production at a detection limit of 1 ppm. The column was heated to 100 °C under He gas flow and the average sample volume of 1 mL was injected onto the column. A 10-mL solution containing the catalyst, photosensitizer, and quencher was added to the cell and sparged with CO_2 for 30 min. Using a three-way valve, the system was closed and the headspace recirculated through the solution continuously during photolysis. A 150 W Xe lamp (Newport Corporation Solar Simulator) fitted with an AM 1.5 filter to mimic the solar spectrum was focused on the solution and the headspace was sampled by the GC every hour. The CO concentration in parts per million was calibrated using pre-mixed CO/N_2 mixtures and the moles were back-calculated from the total headspace volume and the ideal gas law.

Determination of Quantum Efficiency Values. Quantum efficiency (QE) values for the catalytic photoredox reactions were calculated using the following equation:

$$QE = \frac{CO\,molecules \times 2}{Incident\,Photons} * 100\% .$$

The CO concentration in ppm that was detected by the GC was converted to total moles of CO produced using the ideal gas law for our system volume. Because 2 electrons are required to produce one molecule of CO, a factor of 2 was included in the numerator. To determine the flux of incident photons, the average

photon wavelength was estimated to be 500 nm and the flux was calculated from the power measured by a power meter (Melles Griot). From the lamp intensity, measured to be 130 $mW \cdot cm^2$, and the 4.24 cm^2 illuminated area of our bubbler, the incident photon flux was calculated to be 5.00×10^{21} h^{-1}.

Transmission Electron Microscopy. TEM measurements were conducted on samples before and after catalytic photoredox reactions using a Hitachi H-7560 microscope fitted with an Edax Inc, Genesis XM2 HX4851 System Energy Dispersive Spectroscopy (EDS) detector. The special resolution of this TEM is 1 nm along with 0.5% atomic detection limit for the EDS detector. An aliquot of 100 uL of the sample before and after photolysis was drop-casted onto a thin film copper or molybdenum TEM grid. The grid was allowed todry completely before loading into the instrument for measurements.

General Methods for X-Ray Crystallography. Single-crystal X-ray diffraction was conducted at University of California, Berkeley, College of Chemistry, X-Ray Crystallography Facility. Crystals were mounted on nylon loops in paratone-N hydrocarbon oil. All data collections were performed on either a Bruker Quazar or APEX diffractometer equipped with a CCD area detector and a low temperature apparatus. Data integration was performed using SAINT. Preliminary data analysis and absorption correction were performed using XPREP and SADABS. Structure solution and refinement was performed using SHELX software package.

3-(Imidazolyl)isoquinoline (1a). A solution of CuI (0.032 g, 0.17 mmol), *N*-hydroxysuccinimide (0.040 g, 0.35 mmol), and NaOMe (0.255 g, 4.7 mmol) was stirred in 35 mL of DMSO for 15 min in a 150-mL round-bottom pressure flask. Imidazole (3.2 g, 4.7 mmol) and 3-bromoisoquinoline (0.66 g, 3.2 mmol) were added and the flask was sealed and heated to 110 °C for 2 d. Water (25 mL) was added to the brown solution and the mixture was filtered to remove solid particles. The filtrate was then extracted with EtOAc (3 × 50 mL) and the organic layers were combined, washed with water, and dried with Na_2SO_4. The solution was evaporated to dryness and the residue was purified by alumina chromatography using 20% EtOAc/hexanes as the eluent. The final product was a light brown solid (0.25 g, 1.3 mmol, 40%). ^{1}H NMR (500 MHz, $CDCl_3$) δ 9.17 (s, 1H), 8.47 (d, J = 2.0 Hz, 1H), 8.02 (d, J = 8.2 Hz, 1H), 7.88 (d, J = 8.3 Hz, 1H), 7.80 – 7.70 (m, 2H), 7.67 (s, 1H), 7.61 (t, J = 7.5 Hz, 1H), 7.25 (s, J = 1.4 Hz, 1H). ^{13}C NMR (125 MHz, CD_3CN): δ 152.50, 144.71, 137.58, 135.37, 131.58, 130.61, 127.89, 127.72, 127.21, 126.56, 116.52, 107.19. EI-HRMS ($[M]^+$) *m/z* calcd for $C_{12}H_9N_3$ 195.0796, found 195.0800.

1-(Imidazolyl)isoquinoline (2a). A solution of $Pd(OAc)_2$ (0.14 g, 0.6 mmol, 10 mol %), BINAP (0.76 g, 1.2 mmol), NaO*t*Bu (1.0 g, 10 mmol), 1-chloroisoquinoline (1.1 g, 6.1 mmol), and imidazole (0.42 g, 6.2 mmol) was refluxed in 80 mL of degassed toluene for 20 h. The yellow suspension was filtered and evaporated to dryness. The residue was purified by alumina chromatography using 20% EtOAc/hexanes as the eluent and the final product was a yellow solid (0.39 g, 2.0 mmol, 33%). ^{1}H NMR (500 MHz, $CDCl_3$) δ 8.44 (d, J = 5.6 Hz, 1H), 8.09 (s, 1H), 8.04 (d, J = 8.6 Hz, 1H), 7.95 (d, J = 8.2 Hz, 1H), 7.79 (ddd, J = 8.2, 6.9, 1.1 Hz, 1H), 7.74 (d, J = 5.7 Hz, 1H), 7.61 (ddd, J = 8.2, 6.9, 1.1 Hz, 1H), 7.54 (s, 1H), 7.30 (s, 1H). ^{13}C NMR (125 MHz, $CDCl_3$): δ 148.31, 141.24, 138.50, 137.73, 131.18, 129.84, 128.73, 127.28, 124.39, 122.62, 121.43. EI-HRMS ($[M]^+$) *m/z* calcd for $C_{12}H_9N_3$ 195.0796, found 195.0798.

2-(Benzimidazolyl)pyridine (3a). A solution of CuI (0.33 g, 1.7 mmol), *N*-hydroxysuccinimide (0.46 g, 4.0 mmol), and NaOMe (2.20 g, 40 mmol) was stirred in 35 mL of DMSO for 15 min in a 150-mL round-bottom pressure flask. Benzimidazole (3.23 g, 30 mmol) and 2-bromopyridine (2.7 mL, 4.4 g, 28 mmol) were added and the flask was sealed and heated to 110 °C for 18 h. Water (25 mL) was added to the brown solution and the mixture was filtered to remove solid particles. The filtrate was then extracted with EtOAc (3 × 50 mL) and the organics were combined, washed with water, and dried with Na_2SO_4. The solution was evaporated to dryness and the residue was purified by silica chromatography using 2% MeOH/CH_2Cl_2 as the eluent. The final product was a light brown oil (1.63 g, 8.3 mmol, 27%). ^{1}H NMR (500 MHz, $CDCl_3$): δ 8.63 (d, J = 4.5 Hz, 1H), 8.59 (s, 1H), 8.07 (d, J = 7.4 Hz, 1H), 7.95 (t, J = 8 Hz, 1H), 7.88 (d, J = 7.5 Hz, 1H), 7.60 (d, J = 8.1, 1H), 7.43 – 7.34 (m, 2H), 7.32 (dd, J = 4.5, 2.5 Hz, 1H). ^{13}C NMR (125 MHz, $CDCl_3$): δ 149.87, 149.47, 144.68, 141.36, 138.99, 132.13, 124.24, 123.32, 121.88, 120.64, 114.34, 112.68. Anal. Calcd for $C_{12}H_9N_3$: C, 73.83; H, 4.65; N, 21.52. Found: C, 73.41; H, 4.41; N, 21.16. EI-HRMS ($[M]^+$) *m/z* calcd for $C_{12}H_9N_3$ 195.0796, found 195.0800.

Bis(3-(imidazolyl)isoquinolinyl)propane hexafluorophosphate (^{Pr}bimiq1, 1b). A solution of **1a** (0.070 g, 0.36 mmol) and 1,2-dibromopropane (18 μL, 0.026 g, 0.18 mmol) in 8 mL of THF was heated to 100 °C for 2 d in a sealed 35-mL tube pressure flask. White precipitate was collected by vacuum filtration and dissolved in water. Ammonium hexafluorophosphate (0.060 g, 0.37 mmol) was added and the white precipitate was collected by vacuum filtration and washed with EtOH and Et_2O (0.070 g, 0.096 mmol, 54%). ^{1}H NMR (500 MHz, CD_3CN) δ 9.90 (s, 2H), 9.28 (s, 2H), 8.36 (s, 2H), 8.27 – 8.16 (m, 4H), 8.08 (d, *J* = 8.0 Hz, 2H), 7.93 (t, *J* = 7.6 Hz, 2H), 7.82 (t, *J* = 8.6 Hz, 2H), 7.77 (d, *J* = 2.5 Hz, 2H), 4.54 (t, *J* = 7.1 Hz, 4H), 2.73 (quin, *J* = 7.9 Hz, 2H). ^{13}C NMR (125 MHz, CD_3CN): 153.12, 141.54, 136.99, 134.51, 132.62, 129.10, 128.85, 128.23, 127.15, 123.70, 119.74, 110.15, 47.13, 29.64. Anal. Calcd for $C_{27}H_{24}N_6F_{12}P_2$: C, 44.89; H, 3.35; N, 11.63. Found: C, 44.56; H, 3.06; N, 11.45. ESI-HRMS ($[M]^+$) *m/z* calcd for $C_{27}H_{24}N_6\ PF_6$ 577.1699, found 577.1709.

Bis(1-(imidazolyl)isoquinolinyl)propane hexafluorophosphate (^{Pr}bimiq2, 2b). The synthesis of **2b** followed the procedure of **1b**, starting with 0.060 g (0.30 mmol) of **2a**, 16 μL of dibromopropane (0.031 g, 0.15 mmol), and 0.055 g of NH_4PF_6 (0.30 mmol) to yield a white product (0.044 g, 0.061 mmol, 40%). ^{1}H NMR (400 MHz, CD_3CN) δ 9.15 (s, 1H), 8.53 (d, *J* = 5.6 Hz, 2H), 8.21 (d, *J* = 8.2 Hz, 2H), 8.13 (d, *J* = 5.5 Hz, 1H), 8.07 – 7.93 (m, 6H), 7.87 (dd, *J* = 8.6, 6.8 Hz, 2H), 7.79 (t, *J* = 1.9 Hz, 2H), 4.51 (t, *J* = 7.3 Hz, 4H), 2.80 – 2.60 (quin, *J* = 8 Hz, 2H). ^{13}C NMR (125 MHz, CD_3CN): δ 145.23, 140.95, 138.66, 136.71, 132.16, 129.93, 127.70, 124.32, 123.76, 123.10, 122.94, 122.01, 29.92, 29.47. ESI-HRMS ($[M]^+$) *m/z* calcd for $C_{27}H_{24}N_6\ PF_6$ 577.1699, found 577.1712.

Bis(2-(benzimidazoyl)pyridinyl)propane hexafluorophosphate (^{Pr}bbimpy, 3b). The synthesis of **3b** followed the procedure of **1b**, starting with 0.302 g (1.5 mmol) of **3a**, 73 μL of dibromopropane (0.14 g, 0.7 mmol), and 0.252 g of NH_4PF_6 (1.5 mmol) to yield a white product (0.19 g, 0.26 mmol, 34%). ^{1}H NMR (500 MHz, CD_3CN) δ 9.60 (s, 2H), 8.76 (d, *J* = 4.0 Hz, 2H), 8.46 – 8.34 (m, 1H), 8.24 (td, *J* = 7.8, 1.9 Hz, 2H), 8.06-8.02 (m, 2H), 7.89 (d, *J* = 8.2 Hz, 2H), 7.86 – 7.78 (m, 4H), 7.78 – 7.67 (m, 2H), 4.79 (t, *J* = 7.5 Hz, 4H), 2.85 (quin, *J* = 7.5 Hz, 2H). ^{13}C NMR (125 MHz, CD_3CN): δ 149.96, 147.05, 140.62, 131.88, 130.28, 128.35, 127.87, 125.59, 115.92, 113.62, 44.81, 27.95. Anal. Calcd for $C_{27}H_{24}N_6F_{12}P_2$: C, 44.89; H, 3.35; N, 11.63. Found: C, 44.79; H, 3.09; N, 11.51. ESI-HRMS ($[M]^+$) *m/z* calcd for $C_{27}H_{24}N_6PF_6$ 577.1699, found 577.1703.

Bis(2-(benzimidazolylmethyl)pyridinyl)propane hexafluorophosphate (^{Pr}bbimpic, 4b). The synthesis of **4b** followed the procedure of **1b**, starting with 0.17 g (0.82 mmol) of 2-(benzimidazolylmethyl)pyridine, 41 μL of dibromopropane (0.081 g, 0.40 mmol), and 0.134 g of NH_4PF_6 (0.82 mmol) to yield a white product (0.10 g, 0.14 mmol, 34%). ^{1}H NMR (500 MHz, CD_3CN) δ 9.20 (s, 2H), 8.50 (d, *J* = 2.5 Hz, 2H), 7.97 – 7.79 (m, 6H), 7.73-7.68 (m, 4H), 7.60 (d, *J* = 7.8 Hz, 2H), 7.38 (dd, *J* = 7.7, 4.7 Hz, 2H), 5.78 (s, 4H), 4.65 (t, *J* = 7.5 Hz, 4H), 2.70 (quin, *J* = 7.5 Hz, 2H). ^{13}C NMR (125 MHz, CD_3CN): δ 152.23, 149.89, 137.66, 131.81, 131.33, 127.42, 127.32, 124.01, 123.31, 113.96, 113.38, 51.63, 44.29, 28.16. Anal. Calcd for $C_{29}H_{28}N_6F_{12}P_2$: C, 46.41; H, 3.86; N, 11.20. Found: C, 46.33; H, 3.54; N, 11.11. ESI-HRMS ($[M]^+$) *m/z* calcd for $C_{27}H_{24}N_6\ PF_6$ 605.2012, found 605.2014.

[Ni(^{Pr}bimiq1)](PF$_6$)$_2$ (1c). A solution of **1b** (0.044 g, 0.061 mmol) and excess Ag_2O in 4 mL of CH_3CN was stirred for 8 h and the resulting solution was centrifuged to remove fine precipitate. To the colorless filtrate, $Ni(DME)Cl_2$ (0.014 g, 0.064 mmol) was added and stirred for 8 h. The resulting solution was centrifuged and the filtrate was evaporated to obtain a red solid. Salt metathesis was performed by adding $NaPF_6$ (0.010 g, 0.060 mmol) and stirred for 18 h. The resulting solution was centrifuged and the filtrate was evaporated to obtain a yellow solid (0.037 mg, 0.047 mmol, 78%). Single crystals were obtained by diffusing Et_2O into a concentrated solution of **1c** in CH_3CN. ^{1}H NMR (500 MHz, CD_3CN) δ 9.34 (s, 2H), 8.39 (d, *J* = 8.3 Hz, 2H), 8.33 (s, 1H), 8.19 (d, *J* = 8.3 Hz, 2H), 8.10 (t, *J* = 8.2 Hz, 2H), 8.05 (d, *J* = 2.2 Hz, 2H), 7.90 (t, *J* = 8.4, 2H), 7.50 (d, *J* = 2.2 Hz, 1H), 4.41 (br s, 2H), 4.06 (s, 4H), 2.31 (quin, *J* = 5.6 Hz, 2H). ^{13}C NMR (125 MHz, CD_3CN): δ 163.70, 155.21, 14460, 137.80, 135.08, 129.63, 129.25, 127.95, 127.08, 126.27, 107.80, 45.99, 29.66. Anal. Calcd for $C_{27}H_{24}N_6NiF_{12}P_2$: C, 41.62; H, 2.85; N, 10.79. Found: C, 40.05; H, 2.90; N, 10.50. ESI-HRMS ($[M]^+$) *m/z* calcd for $C_{27}H_{24}N_6NiPF_6$ 633.0896, found 633.0911.

[Ni(^{Pr}bimiq2)]$(PF_6)_2$ (2c). The synthesis of **2c** followed the procedure of **1c** with quantitative conversion, starting with 0.035 g (0.048 mmol) of **2b,** 0.011 g (0.050 mmol) of Ni(DME)Cl_2, and 0.008 g (0.048 mmol) of $NaPF_6$ to yield a yellow product. Single crystals were obtained by diffusing Et_2O into a concentrated solution of **2c** in CH_3CN. ^{1}H NMR (500 MHz, CD_3CN) δ 8.65 (d, *J* = 8.7 Hz, 2H), 8.45 (d, *J* = 2.3 Hz, 2H), 8.36 (d, *J* = 6.3 Hz, 2H), 8.24 (d, *J* = 8.3 Hz, 2H), 8.12-8.06 (m, 4H), 7.98 (t, *J* = 7.2, 2H), 7.56 (d, *J* = 2.3 Hz, 1H), 4.40-4.20 (br m, 4H), 2.32 (quin, *J* = 6.0 Hz, 2H). ^{13}C NMR (125 MHz, CD_3CN): δ 162.81, 150.18, 139.88, 139.74, 134.12, 130.88, 126.00, 124.00, 123.16, 121.16, 46.34, 30.18. Anal. Calcd for $C_{27}H_{24}N_6NiF_{12}P_2 \cdot H_2O$: C, 40.68; H, 3.03; N, 10.54. Found: C, 40.36; H, 2.82; N, 10.39. ESI-LRMS ($[M]^+$) *m/z* calcd for $C_{27}H_{24}N_6Ni$ 244.0624, found 244.0626.

[Ni(^{Pr}bbimpy)]$(PF_6)_2$ (3c). A solution of **3b** (0.087 g, 0.12 mmol) and excess Ag_2O in 4 mL of CH_3CN was stirred for 8 h and the resulting solution was centrifuged to remove fine precipitate. To the colorless filtrate, Ni(DME)Cl_2 (0.026 g, 0.12 mmol) was added and stirred for 8 h. The resulting solution was centrifuged and the filtrate was evaporated to obtain a red solid identified by NMR studies and X-ray diffraction as **[Ni(^{Pr}bbimpy)Cl]PF_6 (**0.050 g, 0.08 mmol). Salt metathesis was performed by adding $AgPF_6$ (0.019 g, 0.075 mmol) and stirred for 18 h. The resulting solution was centrifuged and the filtrate was evaporated to obtain a yellow solid (0.065 g, 0.08 mmol, 70% from **3b**). Single crystals were obtained by diffusing Et_2O into a concentrated solution of **3c** in CH_3CN. ^{1}H NMR (500 MHz, CD_3CN) δ 8.55 (d, *J* = 5.4 Hz, 2H), 8.45 (t, *J* = 8.4 Hz, 2H), 8.3 (d, *J* = 8.1, 2H), 8.23 (d, *J* = 7.2 Hz, 2H), 7.88 (d, *J* = 7.8 Hz, 1H), 7.77 – 7.60 (m, 6H), 4.75 (br s, 2H), 4.24 (br s, 2H), 2.42 (quin, *J* = 5.6 Hz, 2H). ^{13}C NMR (125 MHz, CD_3CN): δ 151.24, 150.04, 143.56, 135.16, 130.09, 126.38, 126.11, 124.04, 113.43, 112.69, 112.43, 43.34, 27.51. Anal. Calcd for $C_{27}H_{24}N_6NiF_{12}P_2$: C, 41.62; H, 2.85; N, 10.79. Found: C, 41.83; H, 2.75; N, 11.19. ESI-HRMS ($[M]^+$) *m/z* calcd for $C_{27}H_{24}N_6NiPF_6$ 633.0896, found 633.0915.

[Ni(^{Pr}bbimpic)]$(PF_6)_2$ (4c). The synthesis of **4c** followed the procedure of **1c** with quantitative conversion, starting with 0.10 g (0.16 mmol) of **4b,** 0.035 g (0.16 mmol) of Ni(DME)Cl_2, and 0.027 g (0.16 mmol) of $NaPF_6$ to yield a yellow product. Single crystals were obtained by diffusing Et_2O into a concentrated solution of **4c** in CH_3CN. ^{1}H NMR (500 MHz, CD_3CN) δ 8.36 (d, *J* = 5.6 Hz, 2H), 8.04 (t, *J* = 7.8 Hz, 2H), 7.98-7.95 (m, 4H), 7.71 (d, *J* = 8.3 Hz, 2H), 7.59 (t, *J* = 7.7 Hz, 2H), 7.53 (t, *J* = 7.7 Hz, 2H), 7.32 (t, *J* = 6.5 Hz, 2H), 6.63 (d, *J* = 15.6 Hz, 2H), 6.15 (d, *J* = 21.5 Hz, 2H), 6.08 (d, *J* = 16.0 Hz, 2H), 4.55 (d, *J* = 14.9 Hz, 2H), 3.80 (dt, *J* = 15.5, 7.8 Hz, 2H). ^{13}C NMR (125 MHz, CD_3CN): δ 153.89, 151.97, 141.20, 134.61, 133.05, 125.59, 125.13, 124.94, 124.82, 111.76, 111.32, 51.10, 42.16, 27.21. Anal. Calcd for $C_{29}H_{28}N_6NiF_{12}P_2$: C, 43.15; H, 3.25; N, 10.41. Found: C, 42.88; H, 3.0; N, 10.24. ESI-HRMS ($[M]^+$) *m/z* calcd for $C_{29}H_{26}N_6NiPF_6$ 661.1209, found 661.1223.

Acknowledgments

This work was supported by DOE/LBNL Grant 403801 (C.J.C.) and the Director, Office of Science, Office of Basic Energy Sciences, Materials Sciences and Engineering Division, of the U.S. Department of Energy under Contract No. DE-AC02-05CH11231 (P.Y.). V.S.T. thanks the National Science Foundation for a graduate fellowship and C.G.M. acknowledges the Amgen Scholars Program at UC Berkeley for a summer research fellowship. C.J.C. is an Investigator with the Howard Hughes Medical Institute.

Supporting Information

Additional supplemental figures as labeled in the text, experimental information, and NMR spectra are available in the supporting information. This information is free of charge via the internet at http://pubs.acs.org.

References

(1) Benson, E. E.; Kubiak, C. P.; Sathrum, A. J.; Smieja, J. M. *Chem. Soc. Rev.* **2009**, *38*, 89.
(2) Centi, G.; Perathoner, S. *Catal. Today* **2009**, *148*, 191.
(3) Rakowski Dubois, M.; Dubois, D. L. *Acc. Chem. Res.* **2009**, *42*, 1974.
(4) Cokoja, M.; Bruckmeier, C.; Rieger, B.; Herrmann, W. A.; Kühn, F. E. *Angew. Chem. Int. Ed.* **2011**, *50*, 8510.
(5) Finn, C.; Schnittger, S.; Yellowlees, L. J.; Love, J. B. *Chem. Commun.* **2012**, *48*, 1392.
(6) Schneider, J.; Jia, H.; Muckerman, J. T.; Fujita, E. *Chem. Soc. Rev.* **2012**, *41*, 2036.
(7) Costentin, C.; Robert, M.; Saveant, J.-M. *Chem. Soc. Rev.* **2013**, *42*, 2423.
(8) Collin, J. P.; Sauvage, J. P. *Coord. Chem. Rev.* **1989**, *93*, 245.
(9) Jessop, P. G.; Ikariya, T.; Noyori, R. *Chem. Rev.* **1995**, *95*, 259.
(10) Appel, A. M.; Bercaw, J. E.; Bocarsly, A. B.; Dobbek, H.; DuBois, D. L.; Dupuis, M.; Ferry, J. G.; Fujita, E.; Hille, R.; Kenis, P. J. A.; Kerfeld, C. A.; Morris, R. H.; Peden, C. H. F.; Portis, A. R.; Ragsdale, S. W.; Rauchfuss, T. B.; Reek, J. N. H.; Seefeldt, L. C.; Thauer, R. K.; Waldrop, G. L. *Chem. Rev.* **2013**, *ASAP*
(11) Kumar, B.; Llorente, M.; Froehlich, J.; Dang, T.; Sathrum, A.; Kubiak, C. P. *Annu. Rev. Phys. Chem.* **2012**, *63*, 541.
(12) Windle, C. D.; Perutz, R. N. *Coord. Chem. Rev.* **2012**, *256*, 2562.
(13) Izumi, Y. *Coord. Chem. Rev.* **2013**, *257*, 171.
(14) Hagfeldt, A.; Grätzel, M. *Acc. Chem. Res.* **2000**, *33*, 269.
(15) Alstrum-Acevedo, J. H.; Brennaman, M. K.; Meyer, T. J. *Inorg. Chem.* **2005**, *44*, 6802.
(16) Lewis, N. S.; Nocera, D. G. *Proc. Natl. Acad. Sci. USA* **2006**, *103*, 15729.
(17) Hochbaum, A. I.; Yang, P. *Chem. Rev.* **2009**, *110*, 527.
(18) Gust, D.; Moore, T. A.; Moore, A. L. *Acc. Chem. Res.* **2009**, *42*, 1890.
(19) Sato, S.; Arai, T.; Morikawa, T.; Uemura, K.; Suzuki, T. M.; Tanaka, H.; Kajino, T. *J. Am. Chem. Soc.* **2011**, *133*, 15240.
(20) Sun, L.; Hammarstrom, L.; Akermark, B.; Styring, S. *Chem. Soc. Rev.* **2001**, *30*, 36.
(21) Gray, H. B. *Nat Chem* **2009**, *1*, 112.
(22) Oh, Y.; Hu, X. *Chem. Soc. Rev.* **2013**, *42*, 2253.
(23) Kang, P.; Meyer, T. J.; Brookhart, M. *Chem. Sci.* **2013**, *4*, 3497.
(24) Inoue, T.; Fujishima, A.; Konishi, S.; Honda, K. *Nature* **1979**, *277*, 637.
(25) Aurian-Blajeni, B.; Halmann, M.; Manassen, J. *Solar Energy Materials* **1983**, *8*, 425.
(26) Yoneyama, H.; Sugimura, K.; Kuwabata, S. *J. Electroanal. Chem.* **1988**, *249*, 143.
(27) Ghadimkhani, G.; de Tacconi, N. R.; Chanmanee, W.; Janaky, C.; Rajeshwar, K. *Chem. Commun.* **2013**, *49*, 1297.
(28) Lin, W.; Han, H.; Frei, H. *J. Phys. Chem. B* **2004**, *108*, 18269.
(29) Lin, W.; Frei, H. *J. Am. Chem. Soc.* **2005**, *127*, 1610.
(30) Lin, W.; Frei, H. *C. R. Chimie* **2006**, *9*, 207.
(31) Petit, J.-P.; Chartier, P.; Beley, M.; Deville, J.-P. *J. Electroanal. Chem.* **1989**, *269*, 267.
(32) Barton, E. E.; Rampulla, D. M.; Bocarsly, A. B. *J. Am. Chem. Soc.* **2008**, *130*, 6342.
(33) Kumar, B.; Smieja, J. M.; Kubiak, C. P. *J. Phys. Chem. C* **2010**, *114*, 14220.
(34) Hori, Y.; Wakebe, H.; Tsukamoto, T.; Koga, O. *Electrochim. Acta* **1994**, *39*, 1833.
(35) Kuhl, K. P.; Cave, E. R.; Abram, D. N.; Jaramillo, T. F. *Energy Environ. Sci.* **2012**, *5*, 7050.
(36) Li, C. W.; Kanan, M. W. *J. Am. Chem. Soc.* **2012**, *134*, 7231.
(37) Chen, Y.; Kanan, M. W. *J. Am. Chem. Soc.* **2012**, *134*, 1986.
(38) Chen, Y.; Li, C. W.; Kanan, M. W. *J. Am. Chem. Soc.* **2012**, *134*, 19969.
(39) DiMeglio, J. L.; Rosenthal, J. *J. Am. Chem. Soc.* **2013**, *135*, 8798.
(40) Tornow, C. E.; Thorson, M. R.; Ma, S.; Gewirth, A. A.; Kenis, P. J. A. *J. Am. Chem. Soc.* **2012**, *134*, 19520.

(41) Fisher, B. J.; Eisenberg, R. *J. Am. Chem. Soc.* **1980**, *102*, 7361.
(42) Beley, M.; Collin, J. P.; Ruppert, R.; Sauvage, J. P. *J. Am. Chem. Soc.* **1986**, *108*, 7461.
(43) Collin, J. P.; Jouaiti, A.; Sauvage, J. P. *Inorg. Chem.* **1988**, *27*, 1986.
(44) Balazs, B. G.; Anson, F. C. *J. Electroanal. Chem.* **1992**, *322*, 325.
(45) Fujita, E.; Haff, J.; Sanzenbacher, R.; Elias, H. *Inorg. Chem.* **1994**, *33*, 4627.
(46) Kelly, C. A.; Mulazzani, Q. G.; Venturi, M.; Blinn, E. L.; Rodgers, M. A. J. *J. Am. Chem. Soc.* **1995**, *117*, 4911.
(47) Froehlich, J. D.; Kubiak, C. P. *Inorg. Chem.* **2012**, *51*, 3932.
(48) Hawecker, J.; Lehn, J.-M.; Ziessel, R. *J. Chem. Soc., Chem. Commun.* **1983**, 536.
(49) Bolinger, C. M.; Sullivan, B. P.; Conrad, D.; Gilbert, J. A.; Story, N.; Meyer, T. J. *J. Chem. Soc., Chem. Commun.* **1985**, *0*, 796.
(50) Ishida, H.; Tanaka, K.; Tanaka, T. *Organometallics* **1987**, *6*, 181.
(51) Bolinger, C. M.; Story, N.; Sullivan, B. P.; Meyer, T. J. *Inorg. Chem.* **1988**, *27*, 4582.
(52) Hurrell, H. C.; Mogstad, A. L.; Usifer, D. A.; Potts, K. T.; Abruña, H. D. *Inorg. Chem.* **1989**, *28*, 1080.
(53) Pugh, J. R.; Bruce, M. R. M.; Sullivan, B. P.; Meyer, T. J. *Inorg. Chem.* **1991**, *30*, 86.
(54) Arana, C.; Yan, S.; Keshavarz-K, M.; Potts, K. T.; Abruña, H. D. *Inorg. Chem.* **1992**, *31*, 3680.
(55) Smieja, J. M.; Kubiak, C. P. *Inorg. Chem.* **2010**, *49*, 9283.
(56) Chen, Z.; Chen, C.; Weinberg, D. R.; Kang, P.; Concepcion, J. J.; Harrison, D. P.; Brookhart, M. S.; Meyer, T. J. *Chem. Commun.* **2011**, *47*, 12607.
(57) Bourrez, M.; Molton, F.; Chardon-Noblat, S.; Deronzier, A. *Angew. Chem. Int. Ed.* **2011**, *50*, 9903.
(58) Wang, W.-H.; Hull, J. F.; Muckerman, J. T.; Fujita, E.; Himeda, Y. *Energy Environ. Sci.* **2012**, *5*, 7923.
(59) Hammouche, M.; Lexa, D.; Momenteau, M.; Savéant, J. M. *J. Am. Chem. Soc.* **1991**, *113*, 8455.
(60) Bhugun, I.; Lexa, D.; Savéant, J.-M. *J. Am. Chem. Soc.* **1996**, *118*, 1769.
(61) Costentin, C.; Drouet, S.; Robert, M.; Savéant, J.-M. *Science* **2012**, *338*, 90.
(62) Grodkowski, J.; Neta, P.; Fujita, E.; Mahammed, A.; Simkhovich, L.; Gross, Z. *J. Phys. Chem. A* **2002**, *106*, 4772.
(63) Meshitsuka, S.; Ichikawa, M.; Tamaru, K. *J. Chem. Soc., Chem. Commun.* **1974**, 158.
(64) Lieber, C. M.; Lewis, N. S. *J. Am. Chem. Soc.* **1984**, *106*, 5033.
(65) Kapusta, S.; Hackerman, N. *J. Electrochem. Soc.* **1984**, *131*, 1511.
(66) Ratliff, K. S.; Lentz, R. E.; Kubiak, C. P. *Organometallics* **1992**, *11*, 1986.
(67) Haines, R. J.; Wittrig, R. E.; Kubiak, C. P. *Inorg. Chem.* **1994**, *33*, 4723.
(68) Simon-Manso, E.; Kubiak, C. P. *Organometallics* **2005**, *24*, 96.
(69) Kang, P.; Cheng, C.; Chen, Z.; Schauer, C. K.; Meyer, T. J.; Brookhart, M. *J. Am. Chem. Soc.* **2012**, *134*, 5500.
(70) Angamuthu, R.; Byers, P.; Lutz, M.; Spek, A. L.; Bouwman, E. *Science* **2010**, *327*, 313.
(71) Rail, M. D.; Berben, L. A. *J. Am. Chem. Soc.* **2011**, *133*, 18577.
(72) Seshadri, G.; Lin, C.; Bocarsly, A. B. *J. Electroanal. Chem.* **1994**, *372*, 145.
(73) Barton Cole, E.; Lakkaraju, P. S.; Rampulla, D. M.; Morris, A. J.; Abelev, E.; Bocarsly, A. B. *J. Am. Chem. Soc.* **2010**, *132*, 11539.
(74) Morris, A. J.; McGibbon, R. T.; Bocarsly, A. B. *ChemSusChem* **2011**, *4*, 191.
(75) Richardson, R. D.; Holland, E. J.; Carpenter, B. K. *Nat Chem* **2011**, *3*, 301.
(76) Thoi, V. S.; Chang, C. J. *Chem. Commun.* **2011**, *47*, 6578.
(77) Kirch, M.; Lehn, J.-M.; Sauvage, J.-P. *Helv. Chim. Acta* **1979**, *62*, 1345.
(78) Hori, H.; Johnson, F. P. A.; Koike, K.; Ishitani, O.; Ibusuki, T. *J. Photochem. Photobiol. A: Chem.* **1996**, *96*, 171.

(79) Ogata, T.; Yanagida, S.; Brunschwig, B. S.; Fujita, E. *J. Am. Chem. Soc.* **1995**, *117*, 6708.
(80) Matsuoka, S.; Yamamoto, K.; Ogata, T.; Kusaba, M.; Nakashima, N.; Fujita, E.; Yanagida, S. *J. Am. Chem. Soc.* **1993**, *115*, 601.
(81) Dhanasekaran, T.; Grodkowski, J.; Neta, P.; Hambright, P.; Fujita, E. *J. Phys. Chem. A* **1999**, *103*, 7742.
(82) Ogata, T.; Yamamoto, Y.; Wada, Y.; Murakoshi, K.; Kusaba, M.; Nakashima, N.; Ishida, A.; Takamuku, S.; Yanagida, S. *J. Phys. Chem.* **1995**, *99*, 11916.
(83) Hawecker, J.; Lehn, J.-M.; Ziessel, R. *J. Chem. Soc., Chem. Commun.* **1985**, *0*, 56.
(84) Craig, C. A.; Spreer, L. O.; Otvos, J. W.; Calvin, M. *J. Phys. Chem.* **1990**, *94*, 7957.
(85) Grant, J. L.; Goswami, K.; Spreer, L. O.; Otvos, J. W.; Calvin, M. *J. Chem. Soc., Dalton Trans.* **1987**, *0*, 2105.
(86) Ziessel, R.; Hawecker, J.; Lehn, J.-M. *Helv. Chim. Acta* **1986**, *69*, 1065.
(87) Hirose, T.; Maeno, Y.; Himeda, Y. *J. Mol. Catal. A: Chem.* **2003**, *193*, 27.
(88) Gholamkhass, B.; Mametsuka, H.; Koike, K.; Tanabe, T.; Furue, M.; Ishitani, O. *Inorg. Chem.* **2005**, *44*, 2326.
(89) Bian, Z.-Y.; Sumi, K.; Furue, M.; Sato, S.; Koike, K.; Ishitani, O. *Inorg. Chem.* **2008**, *47*, 10801.
(90) Tamaki, Y.; Morimoto, T.; Koike, K.; Ishitani, O. *Proc. Natl. Acad. Sci. USA.* **2012**, *109*, 15673.
(91) Sato, S.; Morikawa, T.; Kajino, T.; Ishitani, O. *Angew. Chem. Int. Ed.* **2013**, *52*, 988.
(92) Gueymard, C. A.; Myers, D.; Emery, K. *Solar Energy* **2002**, *73*, 443.
(93) Gueymard, C. A. *Solar Energy* **2004**, *76*, 423.
(94) Costamagna, J.; Ferraudi, G.; Canales, J.; Vargas, J. *Coord. Chem. Rev.* **1996**, *148*, 221.
(95) Nicewicz, D. A.; MacMillan, D. W. C. *Science* **2008**, *322*, 77.
(96) Narayanam, J. M. R.; Stephenson, C. R. J. *Chem. Soc. Rev.* **2011**, *40*, 102.
(97) Ischay, M. A.; Yoon, T. P. *Eur. J. Org. Chem.* **2012**, *2012*, 3359.
(98) Hamilton, D. S.; Nicewicz, D. A. *J. Am. Chem. Soc.* **2012**, *134*, 18577.
(99) Creutz, S. E.; Lotito, K. J.; Fu, G. C.; Peters, J. C. *Science* **2012**, *338*, 647.
(100) Prier, C. K.; Rankic, D. A.; MacMillan, D. W. C. *Chem. Rev.* **2013** *113*, 5322
(101) Ma, H.-C.; Jiang, X.-Z. *J. Org. Chem.* **2007**, *72*, 8943.
(102) Xi, Z.; Zhang, X.; Chen, W.; Fu, S.; Wang, D. *Organometallics* **2007**, *26*, 6636.
(103) Zhou, Y.; Xi, Z.; Chen, W.; Wang, D. *Organometallics* **2008**, *27*, 5911.
(104) Gu, S.; Chen, W. *Organometallics* **2009**, *28*, 909.
(105) Kapturkiewicz, A.; Angulo, G. *Dalton Trans.* **2003**, 3907.
(106) Shih, H.-W.; Vander Wal, M. N.; Grange, R. L.; MacMillan, D. W. C. *J. Am. Chem. Soc.* **2010**, *132*, 13600.
(107) Irvine, J. T. S.; Eggins, B. R.; Grimshaw, J. *Solar Energy* **1990**, *45*, 27.
(108) Johne, P.; Kisch, H. *J. Photochem. Photobiol. A: Chem.* **1997**, *111*, 223.
(109) Murov, S. L.; Carmichael, I.; Hug, G. L. *Handbook of Photochemistry*; Marcel Dekker: New York, 1993.
(110) Khan, M. M. T.; Mirza, S.; Bajaj, H. C. *React. Kinet. Catal. Lett.* **1987**, *33*, 67.
(111) Kermagoret, A.; Braunstein, P. *Organometallics* **2007**, *27*, 88.
(112) Connelly, N. G.; Geiger, W. E. *Chem. Rev.* **1996**, *96*, 877.

Schemes, Tables, and Figures

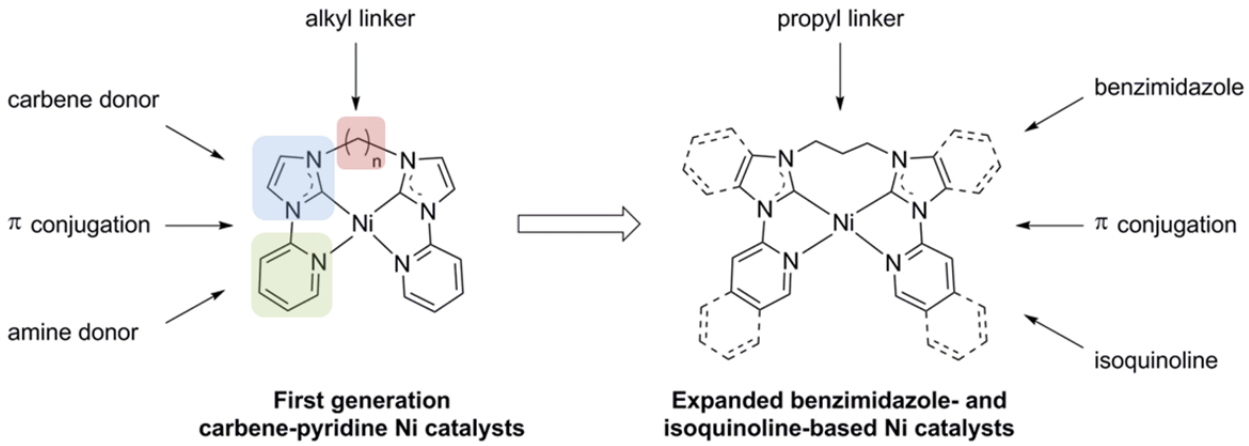

Scheme 1. Ligand design strategy for developing nickel carbene-amine catalysts for CO_2 reduction.

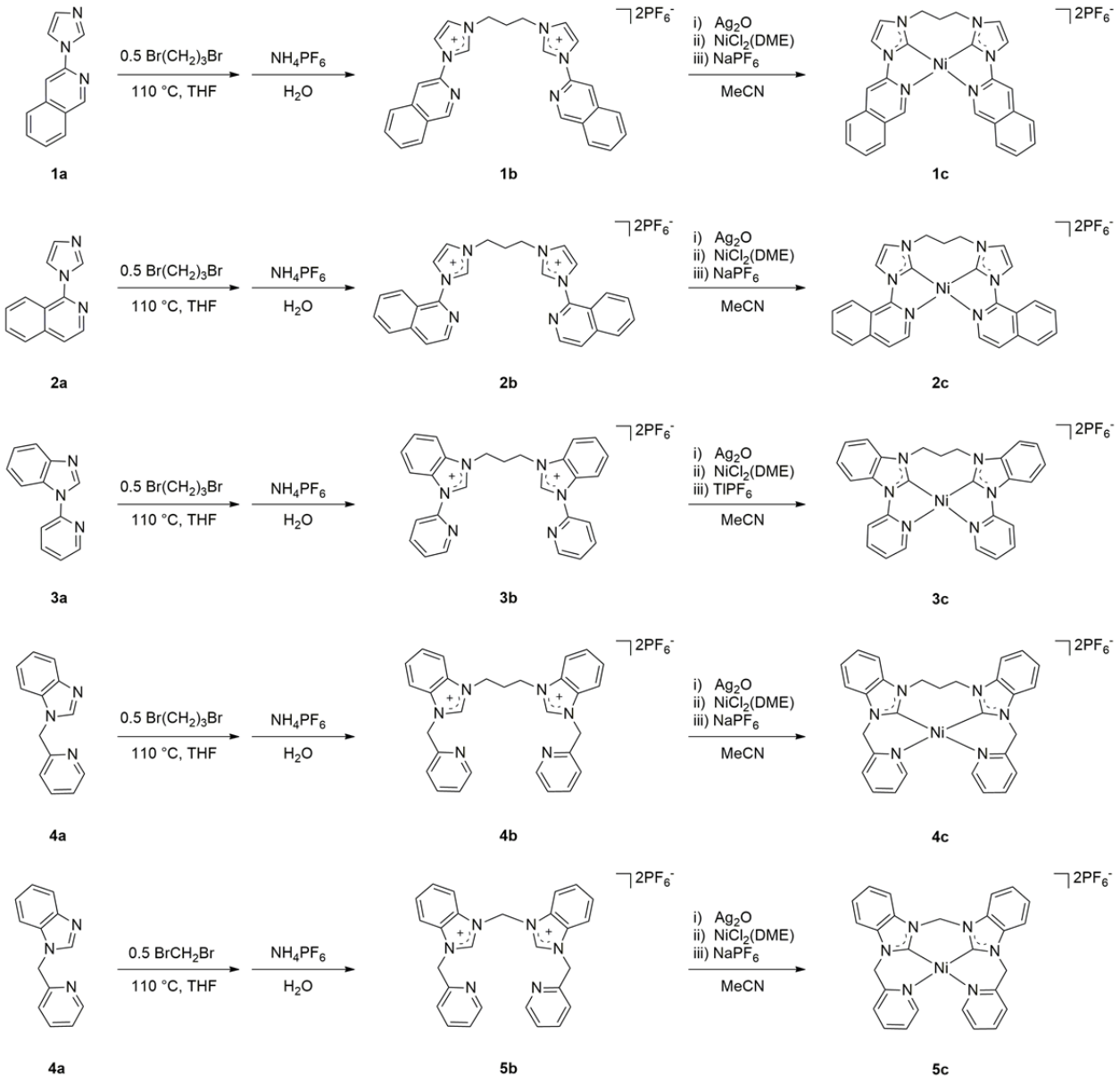

Scheme 2. Synthesis of *N*-heterocyclic carbene-amine ligands **1b**-**5b** and their Ni complexes **1c**-**5c**.

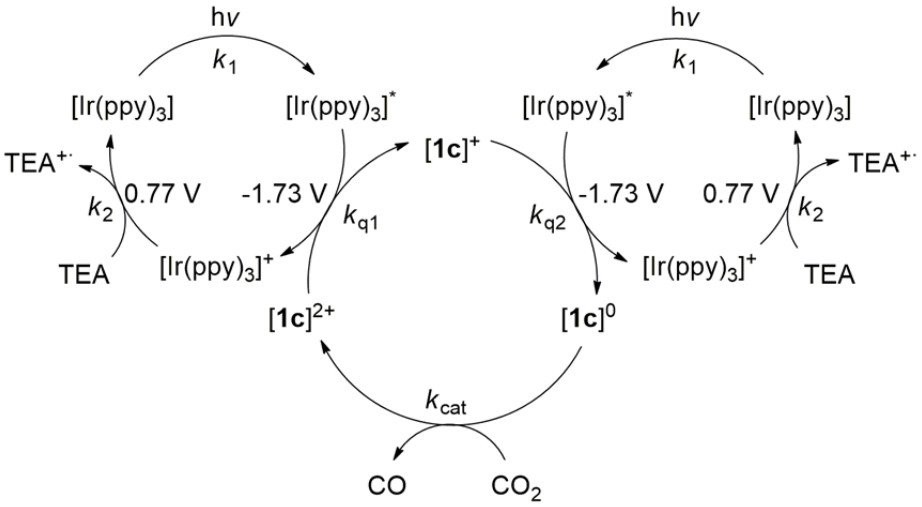

Scheme 3. Proposed photoredox cycle for visible-light-induced reduction of CO_2 to CO. Please note that k_{q1} and k_{q2} are components of the apparent quenching rate, k_q.

Table 1. Turnover numbers (TON) and turnover frequencies (TOF) at various concentrations of catalyst **1c** in an acetonitrile solution containing 0.2 mM $Ir(ppy)_3$ and 0.07 M TEA illuminated with a light intensity of 130 $mW \cdot cm^{-2}$.

[**1c**] (nM)	TON	TOF (s^{-1})
2	98,000	3.9
20	9,000	0.36
200	1,500	0.058

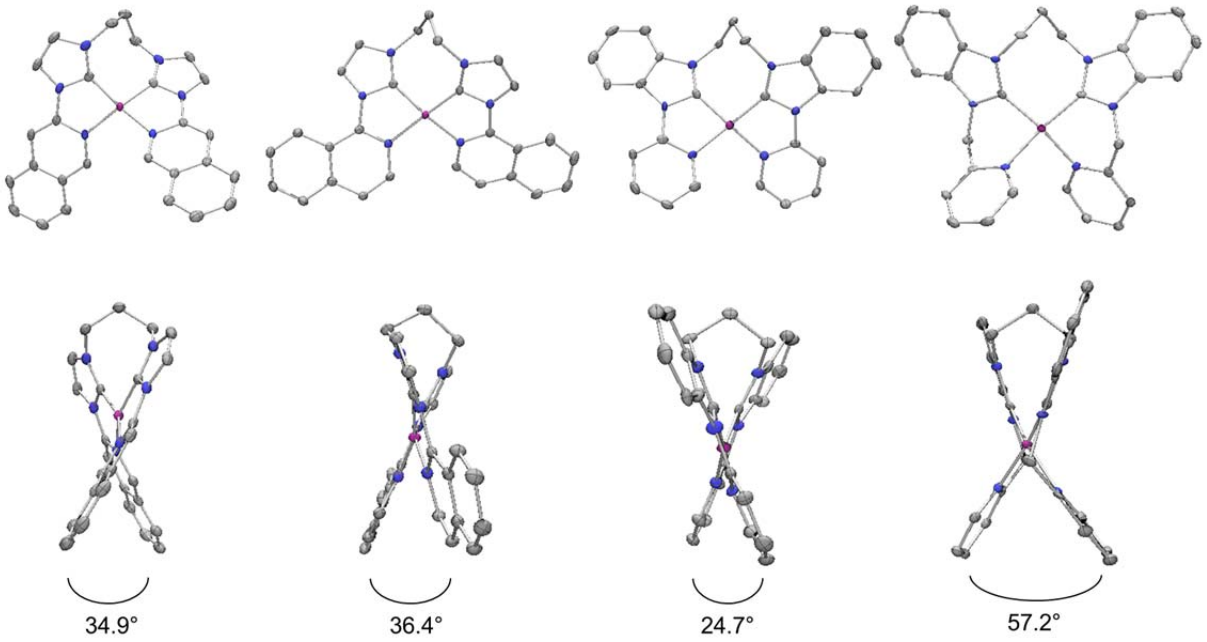

Figure 1. Solid-state structures of **1c**-**4c** (left to right). The top row shows a front view, the bottom row provides a side view highlighting the torsional twist induced by ligand flexibility. Anions, solvent molecules and hydrogen atoms are omitted for clarity; thermal ellipsoids are shown at 50% probability.

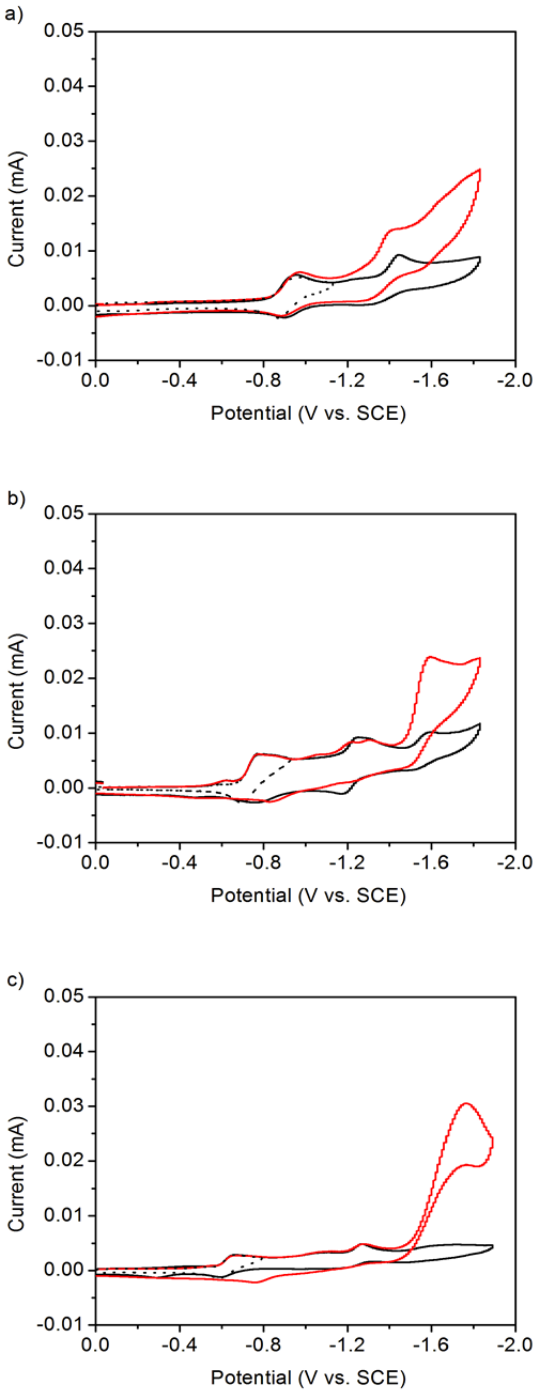

Figure 2. Cyclic voltammograms of complexes a) **1c**, b) **2c**, and c) **3c** in a 0.1 M NBu_4PF_6 acetonitrile solution under a N_2 (black) and CO_2 (red) atmosphere using a glassy carbon disk electrode at a scan rate of 100 $mV \cdot s^{-1}$.

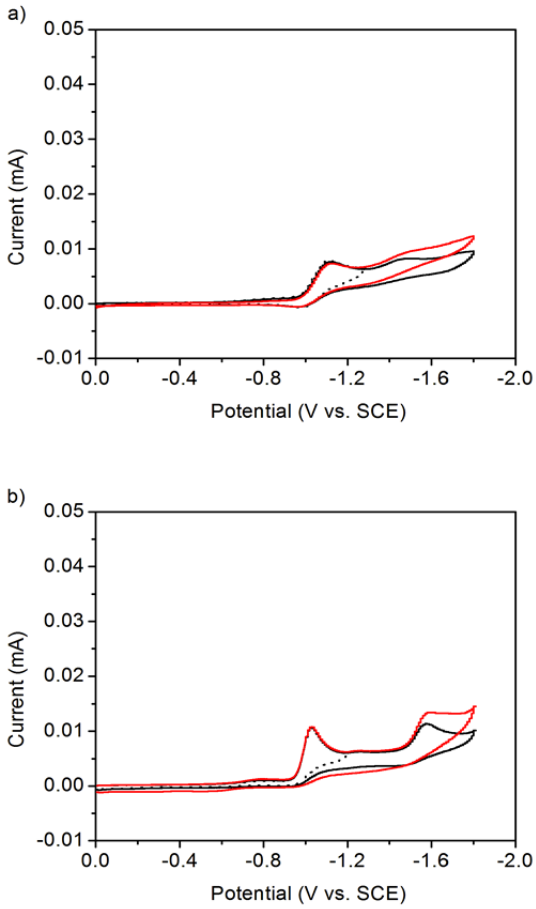

Figure 3. Cyclic voltammograms of complex a) **4c** and b) **5c** in a 0.1 M NBu_4PF_6 acetonitrile solution under a N_2 (black) and CO_2 atmosphere (red) using a glassy carbon disk electrode at a scan rate of 100 $mV \cdot s^{-1}$.

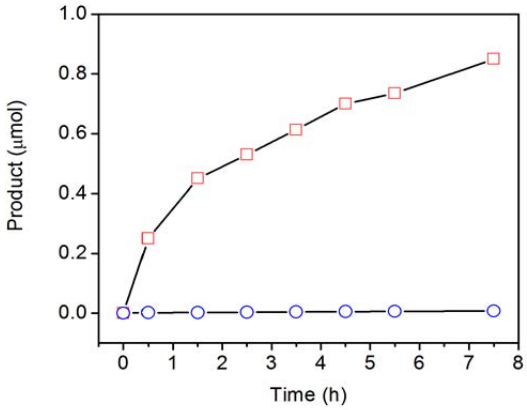

Figure 4. CO (red squares) and CH_4 (blue circles) formation versus electrolysis time in a controlled potential electrolysis in a 0.1 M NBu_4PF_6 acetonitrile solution containing 2 μM **1c** at −1.8 V vs. SCE using a glassy carbon disk electrode under a CO_2 atmosphere.

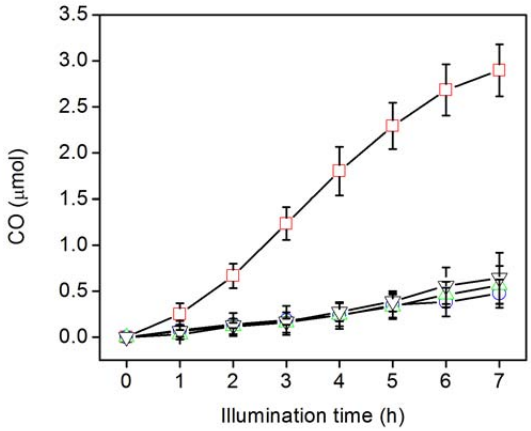

Figure 5. Photocatalytic reduction of CO_2 to CO in a 0.07 M TEA acetonitrile solution containing 0.2 mM $Ir(ppy)_3$ (black triangles), 0.2 μM **1c** (blue circles), 0.2 mM $Ir(ppy)_3$ and 0.2 μM $Ni(CH_3CN)_4(PF_6)_2$ (green triangles), and 0.2 mM $Ir(ppy)_3$ and 0.2 μM **1c** (red squares), using a 130 $mW \cdot cm^{-2}$ Xe lamp fitted with an AM 1.5 filter.

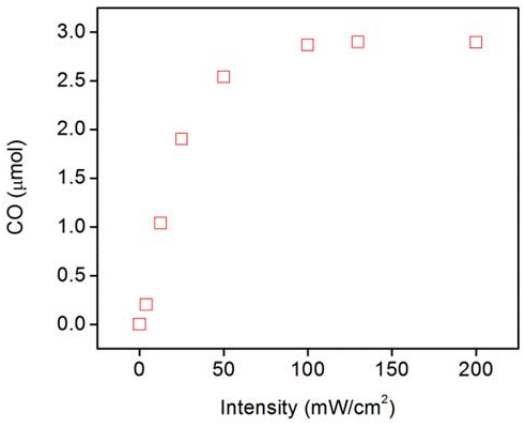

Figure 6. Photocatalytic reduction of CO_2 to CO in a 0.07 M TEA acetonitrile solution containing 0.2 mM $Ir(ppy)_3$ and 0.2 μM **1c** while varying the light intensity of a Xe lamp fitted with an AM 1.5 filter.

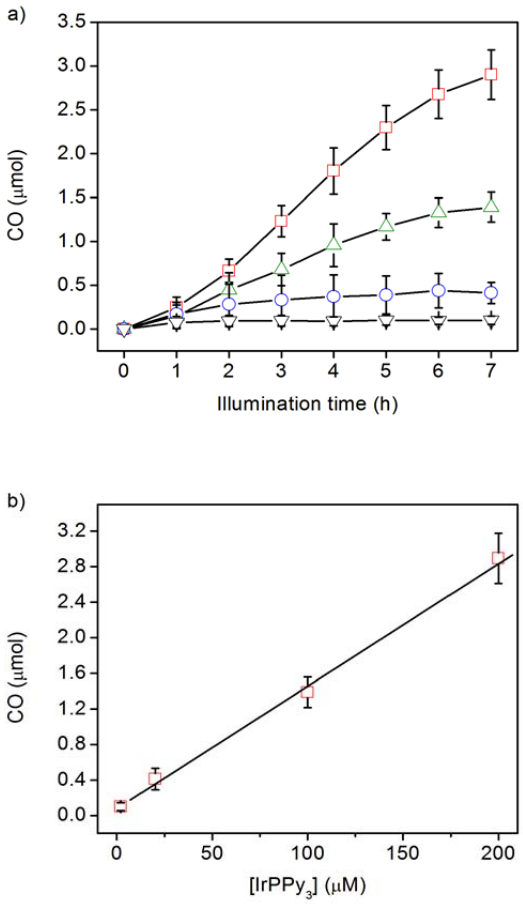

Figure 7. a) Photocatalytic reduction of CO_2 to CO in a 0.07 M TEA acetonitrile solution containing 0.2 μM **1c** and 0.2 mM (red squares), 0.1 mM (green triangles), 0.02 mM (blue circles), and 0.002 mM (black triangles) $Ir(ppy)_3$, using a 130 $mW \cdot cm^{-2}$ Xe lamp fitted with an AM 1.5 filter. b) Linear plot of CO production at the end of 7 h versus $Ir(ppy)_3$ concentration.

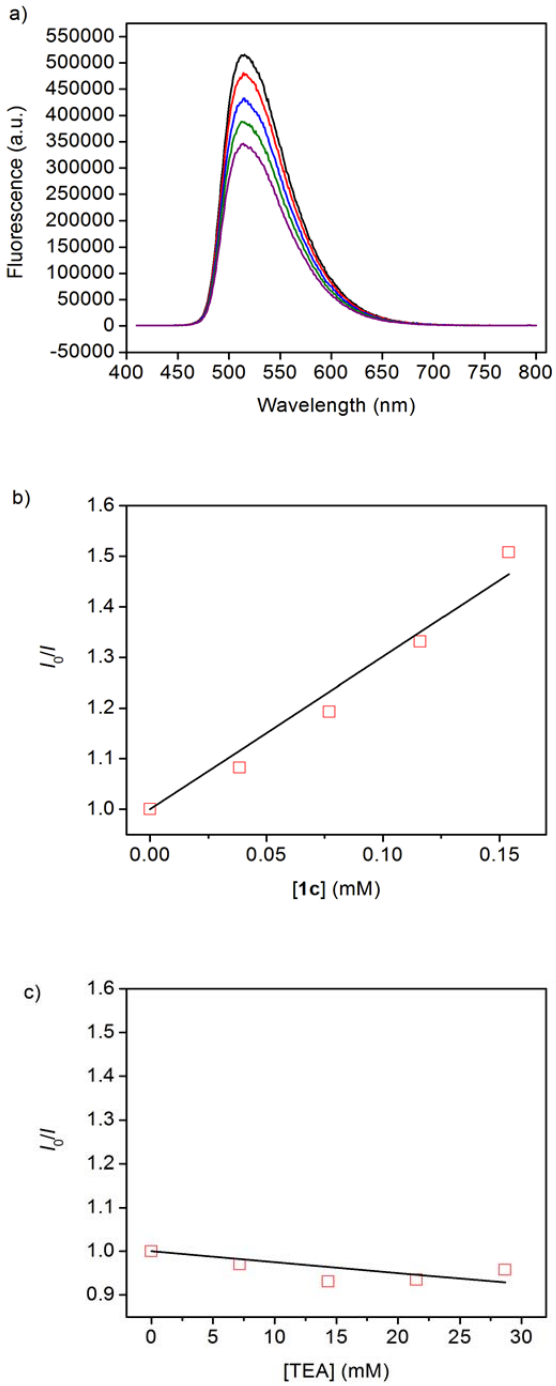

Figure 8. a) Fluorescence spectra of an acetonitrile solution containing 0.05 mM $Ir(ppy)_3$ in the absence (black) and presence of 0.04 mM (red), 0.08 mM (blue), 0.12 mM (green), and 0.15 mM (purple) **1c**. b) Linear plots of ratio of fluorescence intensities in the absence and presence of **1c** versus the concentration of b) **1c** ($y = 3021x + 1$, $R^2 = 0.97$) and c) TEA, according to the Stern-Volmer Equation.

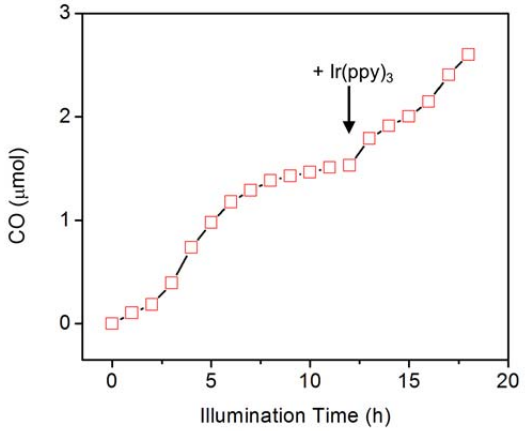

Figure 9. Photocatalytic reduction of CO_2 to CO in a 0.07 M TEA acetonitrile solution containing 0.2 μM **1c** and 0.2 mM $Ir(ppy)_3$, using a 130 $mW \cdot cm^{-2}$ Xe lamp fitted with an AM 1.5 filter. At 13 h, a fresh source of $Ir(ppy)_3$ was injected and CO production was continued.

TOC Graphic

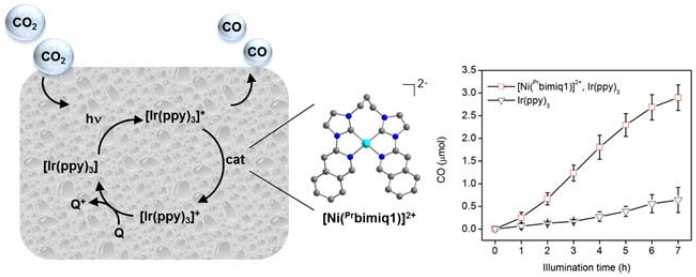
CO2
CO2
CO
CO
hν
[Ir(ppy)3]*
[Ir(ppy)3]
cat
Q+
[Ir(ppy)3]+
Q
2-
[Ni(PrbimiqI)]2+
CO (μmol)
Illumination time (h)
[Ni(PrbimiqI)]2+, Ir(ppy)3
Ir(ppy)3

Acknowledgements: This work was supported by the Director, Office of Science, Office of Basic Energy Sciences, Material Sciences and Engineering Division, of the U.S. Department of Energy under Contract No. DE-AC02-05CH11231. We thank the National Center for Electron Microscopy for the use of their facilities.